Detailed Stress Tensor Measurements in a Centrifugal Compressor Vaneless Diffuser

A. Pinarbasi

M. W. Johnson

Department of Mechanical Engineering,
University of Liverpool,
Liverpool, United Kingdom

Detailed flow measurements have been made in the vaneless diffuser of a large low-speed centrifugal compressor using hot-wire anemometry. The three time mean velocity components and full stress tensor distributions have been determined on eight measurement planes within the diffuser. High levels of Reynolds stress result in the rapid mixing out of the blade wake. Although high levels of turbulent kinetic energy are found in the passage wake, they are not associated with strong Reynolds stresses and hence the passage wake mixes out only slowly. Low-frequency meandering of the wake position is therefore likely to be responsible for the high kinetic energy levels. The anisotropic nature of the turbulence suggests that Reynolds stress turbulence models are required for CFD modeling of diffuser flows.

Introduction

Although the geometry of a vaneless diffuser is simple, the flow is complex due to the highly nonuniform three-dimensional flow, which is inherited from the centrifugal impeller. The features of the impeller outlet flow are well documented (e.g., Johnson and Moore, 1980; Eckardt, 1975; Inoue and Cumpsty, 1984). The flow, whether from a radial discharge or backswept impeller, invariably consists of a jet and a passage wake, although the position and size of the wake are dependent on flow rate and impeller geometry (Johnson and Moore, 1983; Farge and Johnson, 1992). The wake is usually located on the shroud, however, and is of sufficient size to have a strong influence on the diffuser flow. Strong secondary flows that develop in the impeller also persist in the diffuser. This is particularly true in backswept impellers where a strong passage vortex is induced (Krain 1988; Farge and Johnson, 1990). Wakes from the impeller blade trailing edges add to the complexity of the highly nonuniform three-dimensional flow that enters the diffuser.

In the vaneless diffuser, the nonuniformities mix out such that the flow closely resembles a Couette flow between the diffuser walls at the diffuser exit. The blade wakes are observed to mix out very rapidly while the passage wake only mixes out slowly (Inoue and Cumpsty, 1984; Maksoud and Johnson, 1987; Mounts and Brasz, 1992; Pinarbasi and Johnson, 1994). Mixing out is also more pronounced in the circumferential direction than in the axial direction. The Reynolds stresses play a dominant role in the mixing out process in the diffuser. The objective of the current work was to measure the Reynolds stresses in a vaneless diffuser with a view to improving the understanding and hence the modeling of the flow.

Experimental Procedure

A schematic of the low-speed centrifugal compressor rig used in the study is shown in Fig. 1. The impeller was a De Havilland Ghost impeller, the geometry of which is given by Johnson and Moore (1980). In the current study, the original radial outlet section was replaced to provide a 30 deg backswept outlet angle as shown in Fig. 2. The vaneless diffuser has straight walls and a constant cross sectional area. The geometry operating conditions and measurement stations are summarized in Table 1.

Contributed by the International Gas Turbine Institute and presented at the 39th International Gas Turbine and Aeroengine Congress and Exposition, The Hague, The Netherlands, June 13–16, 1994. Manuscript received by the International Gas Turbine Institute February 15, 1995. Paper No. 94-GT-227. Associate Technical Editor: E. M. Greitzer.

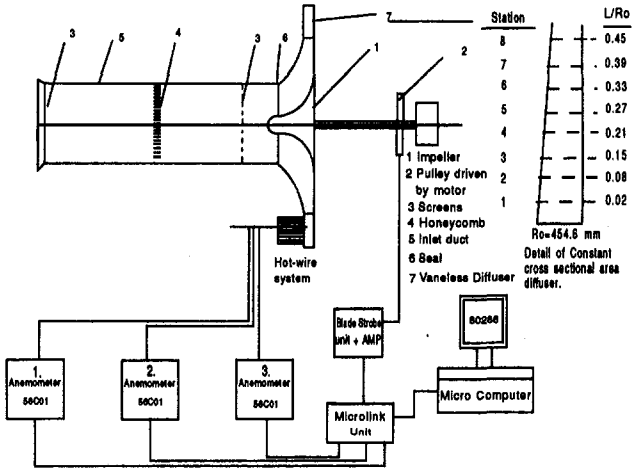


Fig. 1 Schematic of centrifugal compressor test rig

Instrumentation and Measurement Technique

Triple hot wires, which were utilized to measure the velocities within the diffuser, were arranged in a measurement volume of size 5 × 5 × 5 mm. A single wire probe (Dantec 55P11) was aligned circumferentially with a double wire probe (Dantec 55P61) arranged with each wire in the axial radial plane and at 45 deg to both the radial and axial directions. This mutually perpendicular arrangement of wires was therefore capable of

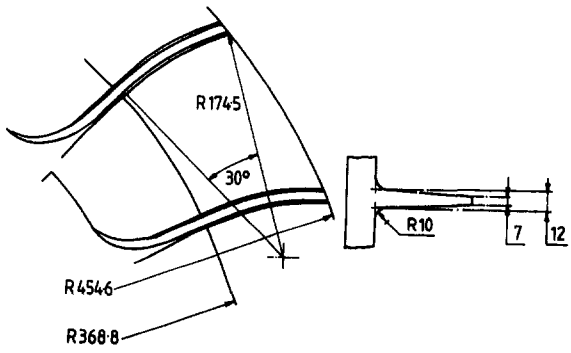


Fig. 2 Backswept impeller blade geometry

Copyright © 1996 by ASME

Downloaded 08 Mar 2011 to 193.140.144.9. Redistribution subject to ASME license or copyright; see http://www.asme.org/terms/Terms_Use.cfm

Table 1 Geometry, operating condition, and measurement locations

Impeller Geometry and Operating Condition:

Inlet blade radius at the hub	R_h = 88.75 mm
Inlet blade radius at the shroud	R_s = 283.75 mm
Outlet radius	R_o = 454.6 mm
Backswept blade angle	β = 30°
Number of the blades	N = 19
Outlet blade span	b = 72.3 mm
Mass flow rate	$\dot{m}$ = 0.142 kg/s
Mean absolute flow angle at diffuser inlet	α = 45°
Rotating speed	n = 500 rpm

Measurement Locations:

Sta.	1	2	3	4	5	6	7	8
L/R_o	0.02	0.08	0.15	0.21	0.27	0.33	0.39	0.45

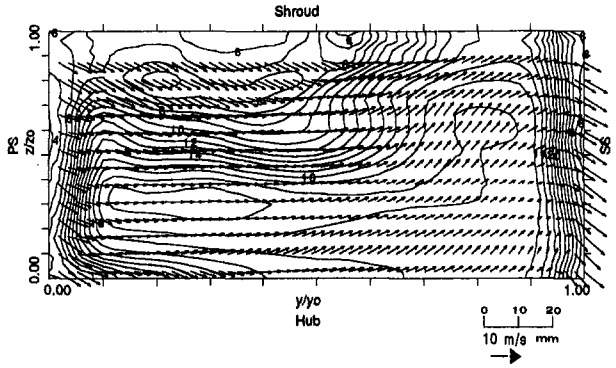


Fig. 3 Mean velocities at Station 1 (L/R_o = 0.02)

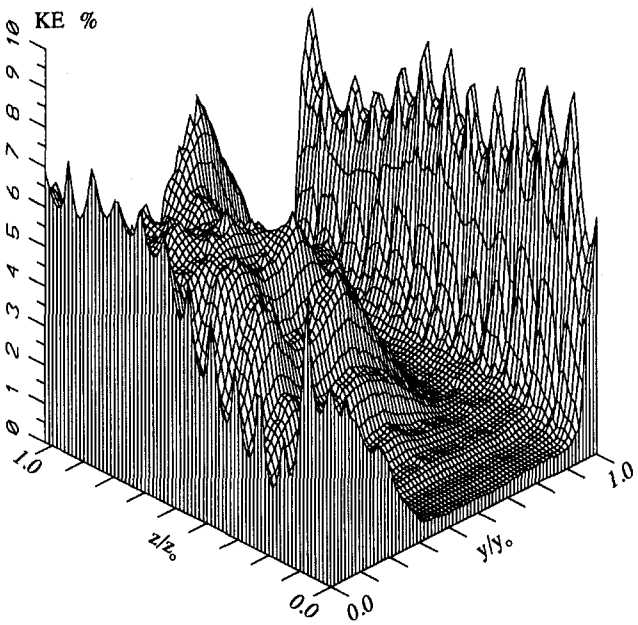


Fig. 4 Turbulent kinetic energy at Station 1 (L/R_o = 0.02)

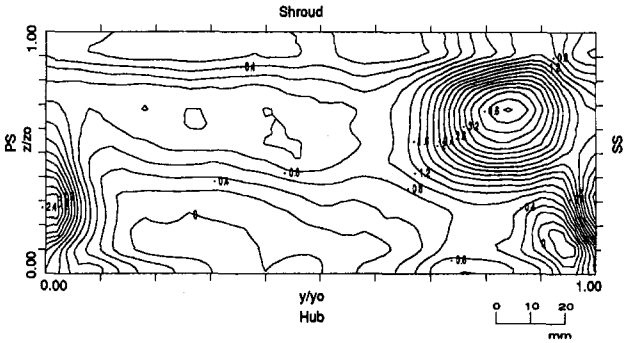


Fig. 5 Reynolds stress $\overline{u_r' u_\theta'}/U_T^2$ (percent): Station 1 (L/R_o = 0.02)

resolving the axial, circumferential, and radial velocity components and the directional sign of the axial component. It was assumed that the radial and circumferential components remained positive throughout the flow. There was no evidence in the results of either of these components reducing to zero and hence this assumption was justified.

The hot wires were connected to three constant-temperature hot-wire anemometer bridges. The wires were then calibrated in two stages in a wind tunnel following the procedure of Jørgensen (1971). In the first stage, the velocity/voltage relationship was established with the wire perpendicular to the flow direction. King's law

$$E^2 = A + B \cdot U_e^c \tag{1}$$

was then fitted to the data for each wire using a least rms error technique to establish the calibration coefficients A, B, and C. The second stage of calibration was achieved by varying the wire orientation at fixed wind tunnel velocity to establish the directional coefficients K and H where

$$U_e^2 = U_n^2 + K \cdot U_t^2 + H \cdot U_b^2 \tag{2}$$

U_n, U_t, and U_b are the normal, tangential, and binormal velocity components relative to the wire. K and H are also obtained by a least rms error curve fitting procedure.

An optical shaft encoder provided a pulse for every $\frac{1}{3}$ deg of impeller rotation. This was used to trigger the simultaneous sampling of the three anemometer voltages through a Microlink data acquisition unit. Readings from 57 measurement points spanning one of the 19 impeller passages were logged on each

Nomenclature

A, B, C = King's law calibration coefficients
E = hot-wire anemometer voltage
H, K = directional coefficients for hot wire
L = radial distance from impeller outlet
R_o = impeller outlet radius
U_T = peripheral blade velocity
U_e = effective cooling velocity
u_θ, u_r, u_z = tangential, radial, and axial mean velocity components
u_θ', u_r', u_z' = tangential, radial, and axial rms fluctuating velocity components
y = tangential coordinate in measurement plane
y_o = tangential distance between consecutive blade wakes
z = axial coordinate in measurement plane
z_o = axial diffuser width in measurement plane

Downloaded 08 Mar 2011 to 193.140.144.9. Redistribution subject to ASME license or copyright; see http://www.asme.org/terms/Terms_Use.cfm

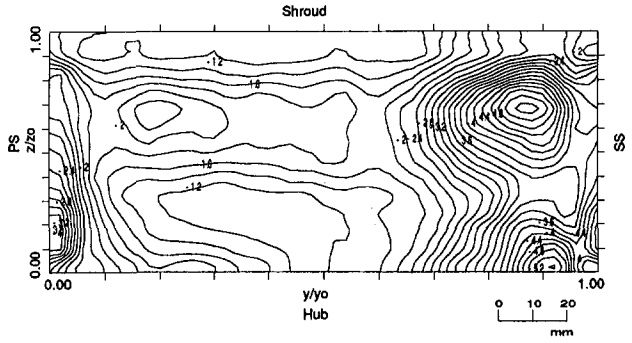


Fig. 6 Reynolds stress $\overline{u_\theta' u_z'}/U_T^2$ (percent): Station 1 (L/R_o = 0.02)

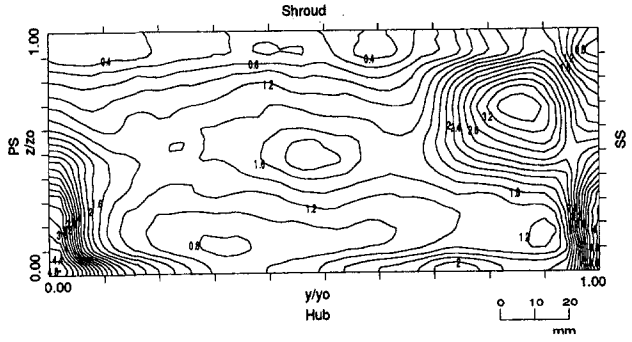


Fig. 7 Reynolds stress $\overline{u_r' u_z'}/U_T^2$ (percent): Station 1 (L/R_o = 0.02)

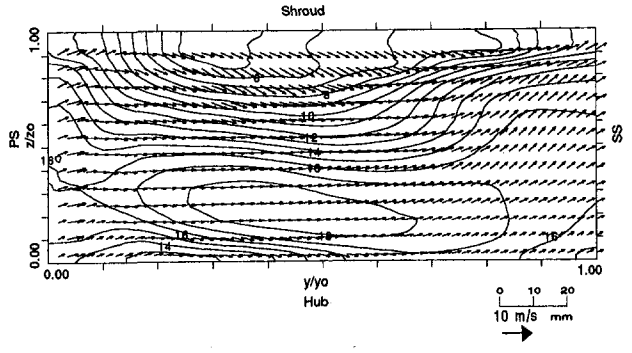


Fig. 8 Mean velocities at Station 2 (L/R_o = 0.08)

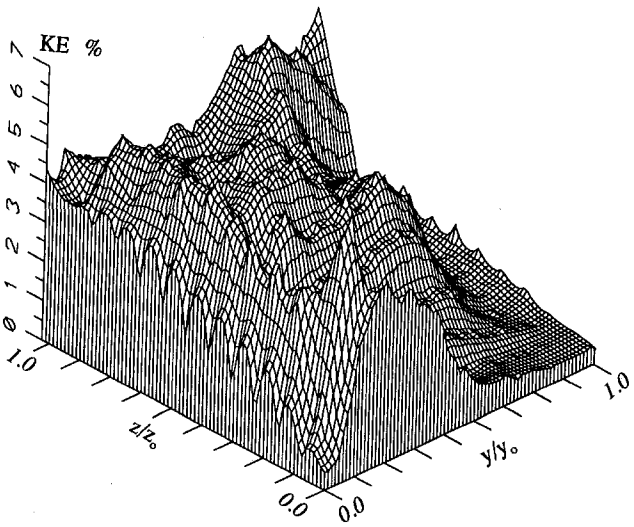


Fig. 9 Turbulent kinetic energy at Station 2 (L/R_o = 0.08)

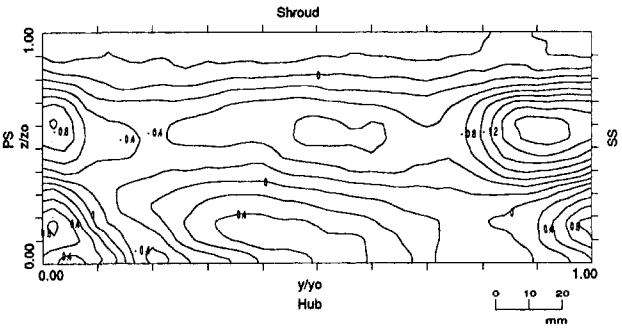


Fig. 10 Reynolds stress $\overline{u_r' u_\theta'}/U_T^2$ (percent): Station 2 (L/R_o = 0.08)

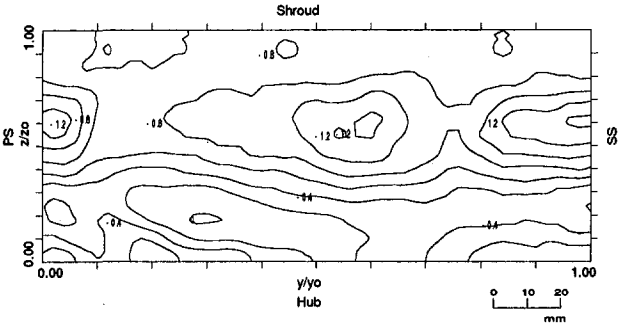


Fig. 11 Reynolds stress $\overline{u_\theta' u_z'}/U_T^2$ (percent): Station 2 (L/R_o = 0.08)

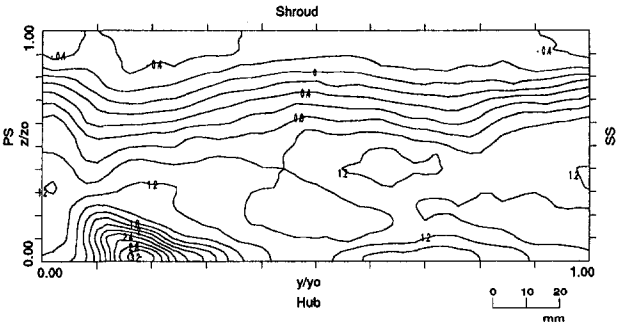


Fig. 12 Reynolds stress $\overline{u_r' u_z'}/U_T^2$ (percent): Station 2 (L/R_o = 0.08)

of 230 consecutive impeller revolutions. The triple wire sensor was traversed in the axial direction in order to provide a mesh of data points for each measurement plane.

Analysis of Results

The 230 readings obtained at each measurement point for each of the three anemometers were used to compute the mean

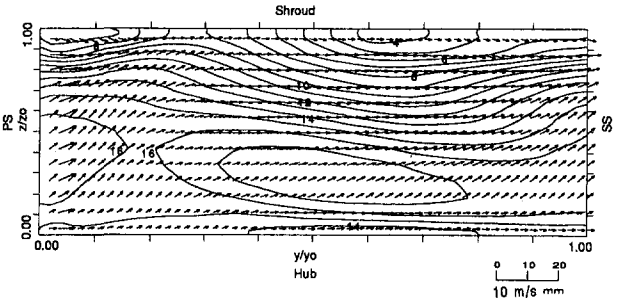


Fig. 13 Mean velocities at Station 3 (L/R_o = 0.15)

Downloaded 08 Mar 2011 to 193.140.144.9. Redistribution subject to ASME license or copyright; see http://www.asme.org/terms/Terms_Use.cfm

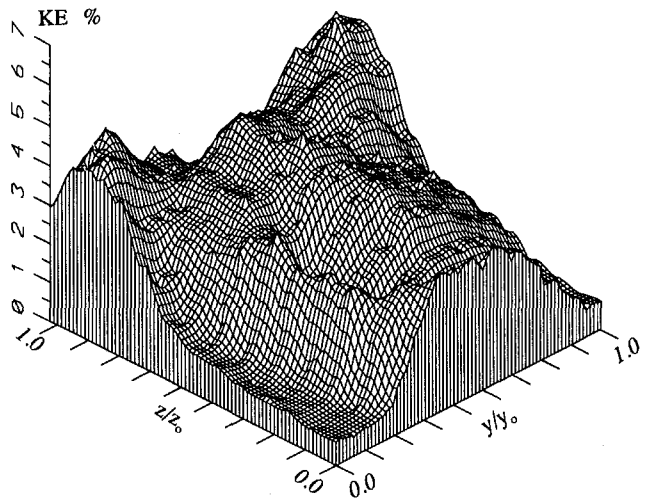


Fig. 14 Turbulent kinetic energy at Station 3 (L/R_o = 0.15)

velocity components and Reynolds stress tensor using the calibration coefficients. The flow rate was also computed by numerical integration of the radial velocity component over each of the measurement planes. The maximum deviation of this flow rate from the mean for all stations was 4.8 percent, which gives an indication of the overall experimental accuracy.

Experimental Results

Station 1. The mean velocities at station 1 are shown in Fig. 3. The radial velocity component is presented as a contour and the remaining velocity in the measurement plane is shown as an arrow. This figure clearly shows the passage wake on the shroud close to the pressure side and the blade wake on the suction side.

Figure 4 shows the turbulent kinetic energy levels at station 1:

$$\frac{\sqrt{(u_r'^2 + u_\theta'^2 + u_z'^2)}}{U_T}$$

The highest levels of around 10 percent are observed in the blade wake, with slightly lower values in the passage wake. It might therefore be expected that the rate of mixing out of the blade and passage wakes would be similar. However, this is not the case as the Reynolds stresses in the passage wake are very much lower than in the blade wake as shown by Figs. 5, 6, and 7. In fact the level of Reynolds stress in the passage wake is similar to that in the majority of the passage where the turbulent kinetic energy is only 1 or 2 percent. It therefore seems likely, as suggested by Hathaway et al. (1993), that the

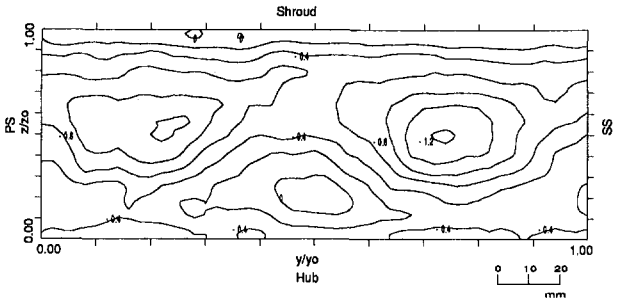


Fig. 16 Reynolds stress $\overline{u_\theta' u_z'}/U_T^2$ (percent): Station 3 (L/R_o = 0.15)

high turbulent kinetic energy level in the wake is due to variations in the position of the wake between impeller revolutions rather than high-frequency turbulent dissipation. The exact position of the wake at the impeller exit is dependent on the opposing secondary flows induced by the impeller axial to radial bend and induced toward the exit of the impeller by Coriolis forces. Quite small changes in the strengths of the secondary flows will therefore lead to variations in the wake position.

The peak levels of Reynolds stress do not in fact occur at the center of the blade wake, but on the suction side of it at $y/y_0 = 0.85$, $z/z_0 = 0.65$. In order to understand the reasons for this, it is necessary to consider the stability of the shear layers within the blade wake, which is governed by the streamline curvature. It has been observed by Bradshaw (1973) that where the shear velocity increases toward the center of curvature, the flow is destabilized as it is in a boundary layer on a concave surface. Conversely, a boundary layer on a convex surface or in a shear layer where the velocity decreases toward the center of curvature is stabilised. In the diffuser, the tangential velocity decreases while the radial velocity is approximately constant, thus the streamline curvature is such that the shear layer on the suction side of the blade is destabilized and that on the pressure side is stabilized. This is consistent with the observation of high levels of Reynolds stress on the suction side of the blade wake with much lower levels of Reynolds stress on the pressure side. Ubaldi et al. (1993) also observed a similar effect on the Reynolds stresses at the exit of their centrifugal pump turbine impeller operated as a pump. In their case however the streamline curvature was in the opposite sense because of the diffuser design.

The relatively different levels of the three components of Reynolds stress indicate that the turbulence is anisotropic. This is particularly true in the hub suction side corner where high levels of $\overline{u_\theta' u_z'}$ stress and low levels of $\overline{u_r' u_\theta'}$ and $\overline{u_r' u_z'}$ stress coexist. This suggests that turbulent eddies (with their axes in the radial direction) exist, which probably originate due to mixing processes within the impeller. However, these eddies are not now associated with large u_r' fluctuations and hence do not lead to significant mixing.

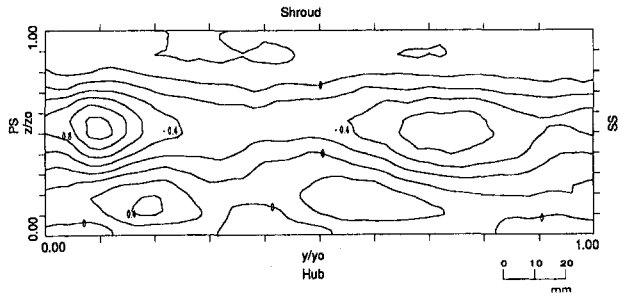


Fig. 15 Reynolds stress $\overline{u_r' u_\theta'}/U_T^2$ (percent): Station 3 (L/R_o = 0.15)

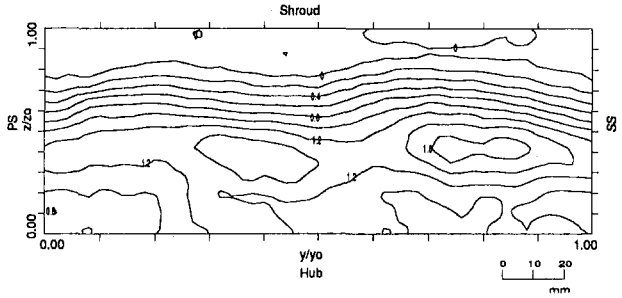


Fig. 17 Reynolds stress $\overline{u_r' u_z'}/U_T^2$ (percent): Station 3 (L/R_o = 0.15)

Downloaded 08 Mar 2011 to 193.140.144.9. Redistribution subject to ASME license or copyright; see http://www.asme.org/terms/Terms_Use.cfm

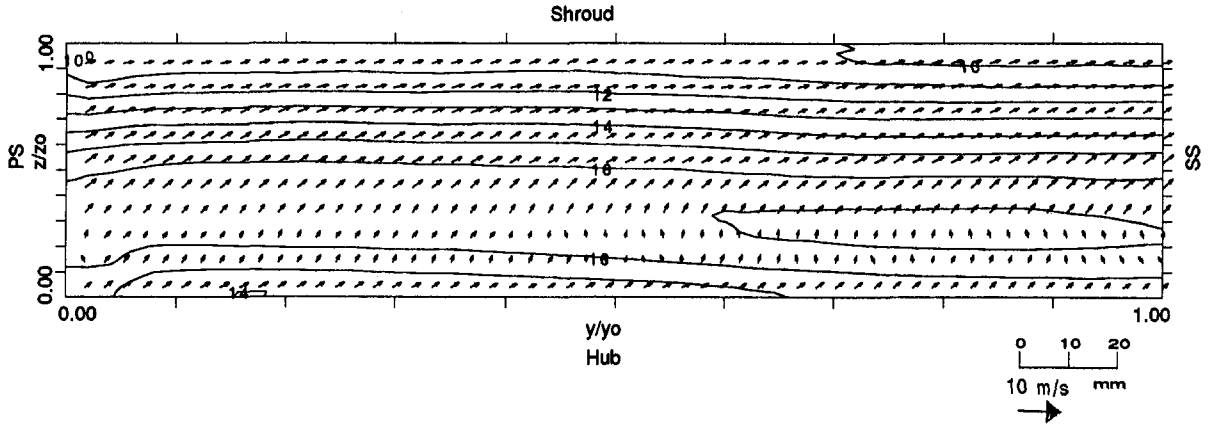


Fig. 18 Mean velocities at Station 8 (L/R_o = 0.45)

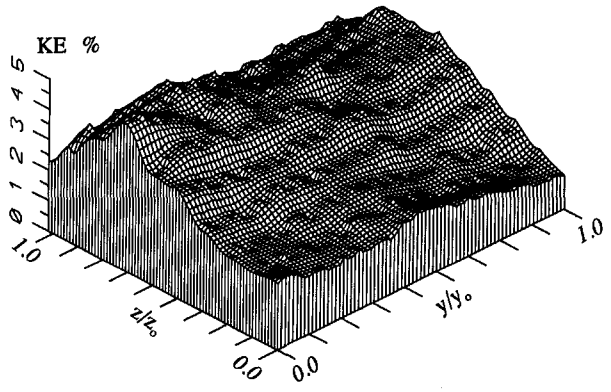


Fig. 19 Turbulent kinetic energy at Station 8 (L/R_o = 0.45)

A further region of mixing occurs near the hub pressure side corner. This appears to be due to destabilizing of the boundary layer on the concave hub surface.

The anisotropic nature of the turbulence suggests that Reynolds stress turbulence models are required for CFD codes used to compute vaneless diffuser flows.

Station 2. Figure 8 shows how the blade wake has largely mixed out and has moved to $y/y_o \approx 0.1$. The kinetic energy and Reynolds stress levels (Figs. 9–12) have all decreased substantially in this region.

The peak level of Reynolds stress occurs in $\overline{u_r' u_z'}$ (Fig. 12) within the blade wake on the hub surface at $y/y_o = 0.2$. This stress is associated with mixing in the boundary layer on the concave hub surface, which is thickened in this region by the blade wake (see Fig. 8). The high level of kinetic energy (Fig. 9) at $y/y_o = 0.9$, $z/z_o = 0.9$ is again due to the meandering of the passage wake across the shroud surface. Even infrequent movement of the wake toward the suction side will result in high levels of kinetic energy due to the large difference in mean velocity between the passage wake (3 m/s) and the main flow (10 m/s). The high level of kinetic energy is not, however, associated with any significant Reynolds stress (Figs. 10, 11, and 12).

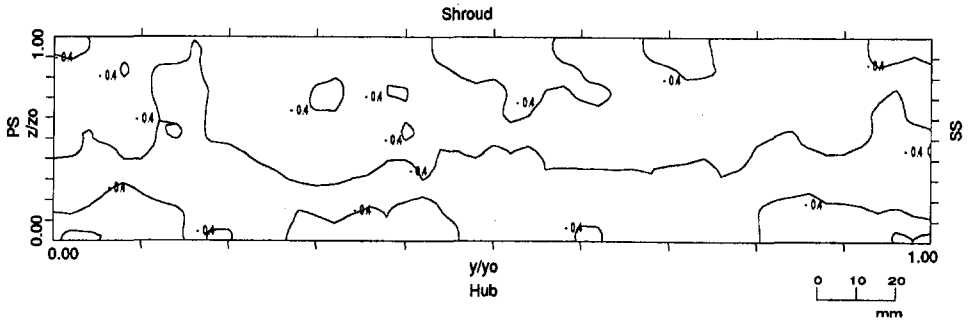


Fig. 20 Reynolds stress $\overline{u_r' u_\theta'}/U_T^2$ (percent): Station 8 (L/R_o = 0.45)

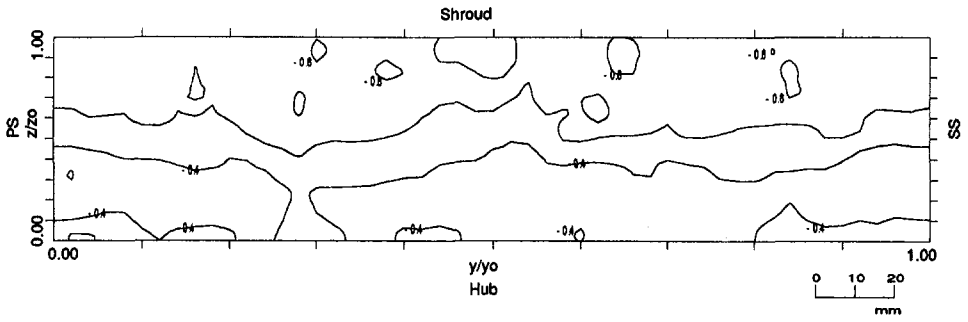


Fig. 21 Reynolds stress $\overline{u_\theta' u_z'}/U_T^2$ (percent): Station 8 (L/R_o = 0.45)

Downloaded 08 Mar 2011 to 193.140.144.9. Redistribution subject to ASME license or copyright; see http://www.asme.org/terms/Terms_Use.cfm

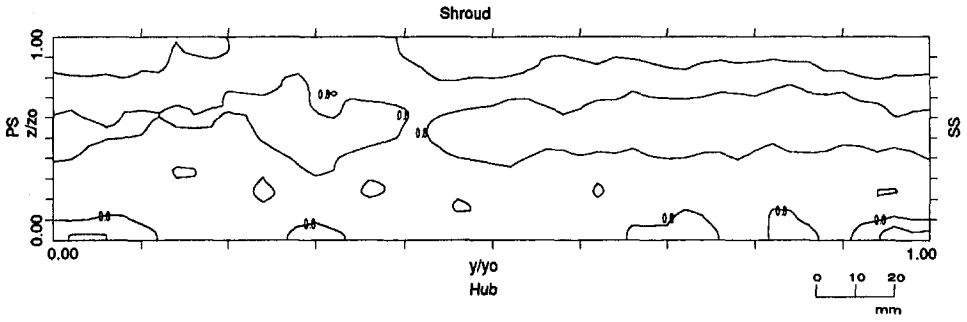


Fig. 22 Reynolds stress $\overline{u_r' u_z'}/U_T^2$ (percent): Station 8 (L/R_o = 0.45)

Station 3. At Station 3 the mean flow (Fig. 13) is beginning to resemble a Couette flow between the hub and shroud walls of the diffuser. The blade wake is still discernible near the hub at $y/y_o \approx 0.3$. The kinetic energy (Fig. 14) also shows a slight increase in this region, however the maximum kinetic energy values are still found on the shroud and are due to meandering of the passage wake. The $\overline{u_r' u_\theta'}$ and $\overline{u_\theta' u_z'}$ Reynolds stress components (Figs. 15 and 16) are now less than the $\overline{u_r' u_z'}$ component (Fig. 17). This would be expected in a Couette flow where mixing is dominated by the hub and shroud wall boundary layers.

Stations 4 to 8. Beyond Station 3, the flow continues to tend toward a Couette flow between the two diffuser walls as shown by the mean velocities at Station 8 (Fig. 18). The passage wake is no longer discernible, although the boundary layer on the shroud surface remains much thicker than that on the hub. The axial velocity from hub to shroud is evidence of the continuing leveling in the two boundary layer flow rates. The peak in turbulent kinetic energy (Fig. 19) is also still located closer to the shroud wall. The levels of all three components of Reynolds stress (Figs. 20, 21, and 22) are now very low, indicating that mixing out of the flow is complete.

Conclusions

1 Turbulent kinetic energy levels and strong Reynolds stresses rapidly mix out the blade wake downstream of the impeller discharge. The Reynolds stresses on the suction side of the blade wake are much larger than those on the pressure side, which is probably due to the effects of streamline curvature on shear layer stability.

2 Although the turbulent kinetic energy levels in the passage wake are as high as those in the blade wake, the Reynolds stresses are very much weaker and hence the passage wake mixes out only slowly. This is consistent with low-frequency turbulent meandering of the passage wake rather than high-frequency turbulent mixing.

3 The diffuser flow eventually develops into a Couette flow between the diffuser walls. The turbulent kinetic energy and Reynolds stress levels at Station 8 suggest that the mixing out of the flow is essentially complete.

4 The Reynolds stress measurements demonstrate that the turbulence is anisotropic. Thus accurate prediction of vaneless diffuser flows will only be possible using Reynolds stress turbulence models in CFD codes.

References

Bradshaw, P., 1973, "Effects of Streamline Curvature on Turbulent Flow," AGARDograph 169.

Eckardt, D., 1975, "Instantaneous Measurements in the Jet-Wake Discharge Flow of a Centrifugal Compressor Impeller," ASME JOURNAL OF ENGINEERING FOR POWER, Vol. 97, pp. 337–346.

Farge, T. Z., and Johnson, M. W., 1990, "The Effect of Backswept Blading on the Flow in a Centrifugal Compressor Impeller," ASME Paper No. 90-GT-231.

Farge, T. Z., and Johnson, M. W., 1992, "Effect of Flow Rate on Loss Mechanisms in a Backswept Centrifugal Impeller," *Int J. Heat Fluid Flow,* Vol. 13, No. 2, pp. 189–196.

Hathaway, M. D., Chriss, R. M., Wood, J. R., and Strazisar, A. J., 1993, "Experimental and Computational Investigation of the NASA Low Speed Centrifugal Compressor Field," ASME JOURNAL OF TURBOMACHINERY, Vol. 115, pp. 527–542.

Inoue, M., and Cumpsty, N. A., 1984, "Experimental Study of the Centrifugal Impeller Discharge Flow in Vaneless Diffusers," ASME *Journal of Engineering for Gas Turbines and Power,* Vol. 106, pp. 455–467.

Johnson, M. W., and Moore, J., 1980, "The Development of Wake Flow in a Centrifugal Compressor," ASME *Journal of Engineering for Power,* Vol. 102, pp. 383–390.

Johnson, M. W., and Moore, J., 1983, "Influence of Flow Rate on the Wake in a Centrifugal Impeller," ASME *Journal of Engineering for Power,* Vol. 105, pp. 33–39.

Jørgensen, F. E., 1971, "Directional Sensitivity of Wire and Fibre Film Probes," DISA information No. 11, pp. 31–37.

Krain, M., 1988, "Swirling Impeller Flow," ASME JOURNAL OF TURBOMACHINERY, Vol. 110, pp. 122–128.

Maksoud, T. M. A., and Johnson, M. W., 1987, "Mean and Turbulent Flow Measurements Within the Vaneless Diffuser of a Centrifugal Compressor," *Proc. IMechE Conf.,* C263/87.

Mounts, J. S., and Brasz, J. J., 1992, "Analysis of the Jet/Wake Mixing in a Vaneless Diffuser," ASME Paper No. 92-GT-418.

Pinarbasi, A., and Johnson, M. W., 1994, "Detailed Flow Measurements in a Centrifugal Compressor Vaneless Diffuser," ASME JOURNAL OF TURBOMACHINERY, Vol. 116, pp. 453–461.

Ubaldi, M., Zunino, P., and Cattanei, A., 1993, "Relative Flow and Turbulence Measurements Downstream of a Backward Centrifugal Impeller," ASME JOURNAL OF TURBOMACHINERY, Vol. 115, pp. 543–551.

Downloaded 08 Mar 2011 to 193.140.144.9. Redistribution subject to ASME license or copyright; see http://www.asme.org/terms/Terms_Use.cfm